nature COMMUNICATIONS

ARTICLE

Received 4 Jun 2014 | Accepted 16 Feb 2015 | Published 26 Mar 2015

DOI: 10.1038/ncomms7653

The transcription factor Foxc1 is necessary for Ihh–Gli2-regulated endochondral ossification

Michiko Yoshida[1,2,*], Kenji Hata[1,*], Rikako Takashima[1], Koichiro Ono[1], Eriko Nakamura[1], Yoshifumi Takahata[1], Tomohiko Murakami[1], Sachiko Iseki[3], Teruko Takano-Yamamoto[2], Riko Nishimura[1] & Toshiyuki Yoneda[1,4]

Indian hedgehog (Ihh) regulates endochondral ossification in both a parathyroid hormone-related protein (PTHrP)-dependent and -independent manner by activating transcriptional mediator Gli2. However, the molecular mechanisms underlying these processes remain elusive. Here by using *in vivo* microarray analysis, we identify forkhead box C1 (Foxc1) as a transcriptional partner of Gli2. Foxc1 stimulates expression of Ihh target genes, including PTHrP and Col10a1, through its physical and functional interaction with Gli2. Conversely, a dominant negative Foxc1 inhibits the Ihh target gene expression. In a spontaneous loss of Foxc1 function mouse ($Foxc1^{ch/ch}$), endochondral ossification is delayed and the expression of Ihh target genes inhibited. Moreover, the pathological Foxc1 missense mutation observed in the Axenfeld–Rieger syndrome impairs Gli2–Foxc1 association as well as Ihh function. Our findings suggest that Foxc1 is an important transcriptional partner of Ihh–Gli2 signalling during endochondral ossification, and that disruption of the Foxc1–Gli2 interaction causes skeletal abnormalities observed in the Axenfeld–Rieger syndrome.

[1] Department of Molecular and Cellular Biochemistry, Osaka University Graduate School of Dentistry, 1-8 Yamadaoka, Suita 565-0871, Japan. [2] Division of Orthodontics and Dentofacial Orthopedics, Tohoku University Graduate School of Dentistry, 4-1 Seiryo-machi, Aoba-ku, Sendai 980-8575, Japan. [3] Section of Molecular Craniofacial Embryology, Graduate School of Medical and Dental Sciences, Tokyo Medical and Dental University, 1-5-45 Yushima, Bunkyo-ku, Tokyo 113-8549, Japan. [4] Division of Hematology/Oncology, Indiana University School of Medicine, Walther Hall, R3-C321D, 980 West Walnut Street, Indianapolis, Indiana 46202, USA. * These authors contributed equally to this work. Correspondence and requests for materials should be addressed to K.H. (email: hata@dent.osaka-u.ac.jp) or to R.N. (email: rikonisi@dent.osaka-u.ac.jp).

Skeletal development occurs via two independent biological processes known as intramembranous ossification and endochondral ossification[1]. During intramembranous ossification, mesenchymal stem cells differentiate into osteoblasts that produce and mineralize bone matrix without cartilage template. The clavicle and flat bones, including calvaria, mandible and maxilla, are formed by intramembranous ossification[2,3]. In contrast, endochondral ossification is mainly conducted by chondrocytes and involves sequential steps of chondrocyte differentiation followed by the replacement of bone[4]. During early stage chondrocyte differentiation, mesenchymal cells condense and differentiate into resting and proliferating chondrocytes that produce abundant extracellular matrix, including type-2 collagen and aggrecan[5]. In the late stage, proliferating chondrocytes become hypertrophic chondrocytes that produce type-10 collagen and matrix metalloproteinase (MMP)-13 (ref. 4). Finally, the hypertrophic chondrocytes undergo apoptosis, which is followed by the invasion of blood vessels and osteoblasts[6]. In humans, most long bones and some craniofacial bones, including the mandibular condyle and sphenoid bone, are formed by endochondral ossification. Thus, the impairment of endochondral ossification causes various skeletal abnormalities, including a short stature and facial dysmorphism[7].

Different cytokines, growth factors and hormones regulate endochondral ossification by activating intracellular signalling molecules and transcription factors. Bone morphogenetic protein family members control chondrocyte proliferation and matrix synthesis by activating Smads[8,9]; cartilage-specific deletion of Smad1/5 in mice results in severe chondrodysplasia[10]. Indian hedgehog (Ihh), a member of the hedgehog family, plays critical roles in the endochondral ossification via its regulation of genes, such as parathyroid hormone-related protein (*PTHrP*), protein patched homologue 1 (*Ptch1*), α1(X) collagen (*Col10a1*) and *Gli1*, by activating the transcription factor Gli2 (refs 11–14). The deletion of *Ihh* or *Gli2* causes severe skeletal defects with reduced chondrocyte proliferation and maturation[15–17]. In addition, Sex-determining region Y-type high mobility group box protein 9 (Sox9) and Runt-related transcription factor 2/3 (Runx2/3), are critical transcription factors for early chondrogenesis[18] and chondrocyte hypertrophy[19].

The transcriptional machineries of individual genes assemble into transcriptional networks that orchestrate the complicated but well-organized chondrocyte differentiation steps during endochondral ossification[20]. Thus, the identification and characterization of novel transcription factors involved in these processes will contribute to a better understanding of endochondral ossification. Numerous attempts have been made to identify these and we previously identified several transcription factors using a high-throughput assay system[21–24] and Solexa deep-sequencing technology[25]. However, the transcriptional networks of endochondral ossification are still not fully elucidated.

In this study, we established a gene-screening system to identify novel transcription factors involved in endochondral ossification using a combination of chondrocyte reporter mice and flow cytometry (fluorescence-activated cell sorting, FACS)-assisted microarray analysis. This revealed that forkhead box c1 (Foxc1) plays a critical role in endochondral ossification through its physical and functional association with Ihh–Gli2 signalling. We also established that the loss of interaction caused by a missense mutation in *Foxc1* partially accounts for pathogenesis of the abnormal skeletal development observed in the Axenfeld–Rieger syndrome. Our findings provide new insights into the transcriptional network system that is critical for endochondral ossification and demonstrate a pathogenic mechanism of skeletal abnormalities in the Axenfeld–Rieger syndrome.

Results

Identification of genes selectively expressed in cartilage. We first attempted to identify transcription factors that were highly expressed in developing cartilage during the embryonic stage. In particular, we aimed to isolate transcription factors relevant to the *in vivo* situation. We, therefore, generated transgenic mice in which the chondrocytes were fluorescently labelled with the Venus gene expression reporter driven by the *Col2a1* promoter (*Col2a1*-Venus-Tg; Supplementary Fig. 1a). Exogenous expression of Venus in cartilage tissues of *Col2a1*-Venus-Tg mice was confirmed by fluorescence stereomicroscopy (Supplementary Fig. 1b,c). Cartilage from the limbs, rib cages and vertebrae of E13.5 *Col2a1*-Venus-Tg mice was dissociated and digested into single cells using collagenase and trypsin (Supplementary Fig. 1d).

Venus-negative and -positive cells were sorted using FACS Aria, and RNA was isolated from each population without cell expansion (Supplementary Fig. 1d). Reverse transcription polymerase chain reaction (RT–PCR) analysis demonstrated that the Venus gene was only expressed in Venus-positive cells (Supplementary Fig. 1e). We purified 2.0 μg total RNA from Venus-negative cells and 1.75 μg total RNA from Venus-positive cells and subjected it to microarray analysis using an Affymetrix Mouse Genome 430 2.0 Array. High chondrocyte gene expression was observed in Venus-positive cells by quantitative RT–PCR (RT–qPCR; Fig. 1a) and microarray analysis (Supplementary Table 1), indicating that purification of chondrocytes and gene expression profiling was successful. Microarray analysis, focusing on transcription factors, also showed that Sox5, Sox6 and Sox9 were highly expressed in Venus-positive cells (Table 1). From the 10 most highly expressed transcription factors shown in Table 1, we selected Foxc1 as a suitable candidate because human *FOXC1* mutations cause the Axenfeld–Rieger syndrome, which is characterized by skeletal abnormalities[26,27]. However, the role of Foxc1 in chondrogenesis is unknown. Venus-positive cells expressed a high level of Foxc1, (1284) similar to that for Sox9 (1601; Table 1) and *Foxc1* expression was increased by 7.03-fold compared with Venus-negative cells (Fig. 1b).

Expression of Foxc1 in chondrocytes. We next used RT–qPCR to demonstrate high levels of *Foxc1* expression in the sternum and rib cartilage, where *Col2a1* is also highly expressed (Fig. 1c). Whole-mount *in situ* hybridization analysis of E12.5 mice revealed high *Foxc1* expression in developing limb buds (Fig. 1d) and *in situ* hybridization analysis of E15.5 mouse tibias showed strong expression of *Foxc1* in *Col2a1*-positive chondrocytes (Fig. 1e). Importantly, *Foxc1* mRNA was detected in distal chondrocytes, which are known to produce PTHrP (Fig. 1e). Immunohistochemical analysis of E13.5 developing limb buds also demonstrated that Foxc1 was detected not only in proliferating chondrocytes but also in perichondrial cells at the end of growth plates where PTHrP is synthesized (Supplementary Fig. 2a). Moreover, Foxc1 was expressed in resting, proliferating and hypertrophic chondrocytes in the tibial growth plates of newborn mice (Supplementary Fig. 2b). These data collectively suggest that Foxc1 might play multifunctional roles during both early and late endochondral ossification.

Foxc1 is critical for endochondral ossification *in vivo*. Using a spontaneous loss of Foxc1 function mutant mouse ($Foxc1^{ch/ch}$), we determined the *in vivo* significance of Foxc1 during endochondral ossification. $Foxc1^{ch/ch}$ mice died soon after birth and showed abnormal skeletal development, as previously described[28]. Skeletal preparations of newborn $Foxc1^{ch/ch}$ mice showed a reduction in Alcian Blue staining, no ossification centre in the

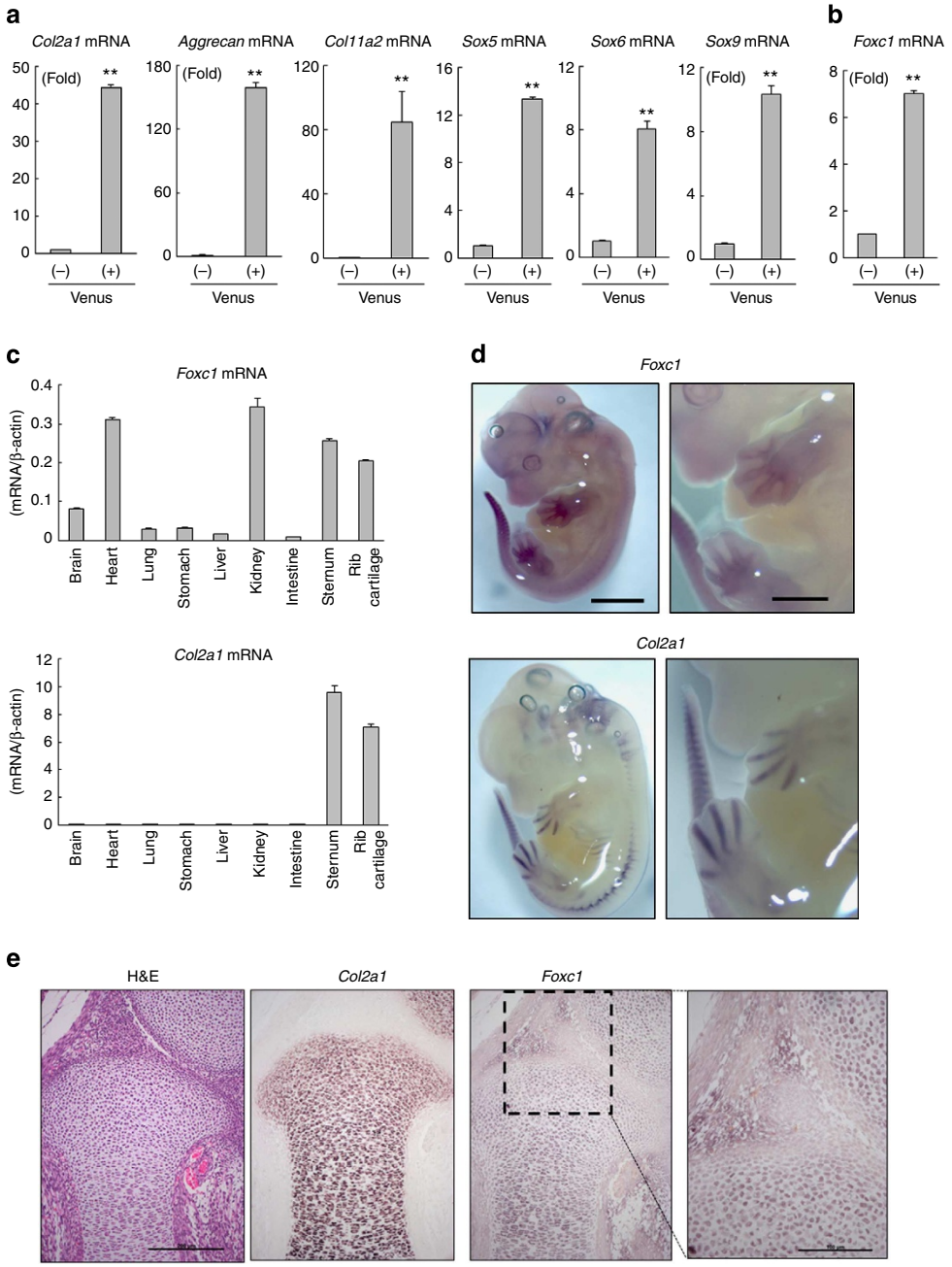

Figure 1 | Identification of Foxc1 as a candidate transcription factor selectively expressed in chondrocytes. (**a**,**b**) Total RNA isolated from Venus-negative and -positive cells was analysed by RT-qPCR for chondrocyte marker genes (**a**) and *Foxc1* (**b**) expression. Data are shown as the mean ± s.d. ($n = 3$). $^{**}P < 0.01$ (versus Venus (−)); Student's *t*-test. (**c**) Tissue distribution of *Foxc1* (upper panel) and *Col2a1* (lower panel) mRNA in newborn mouse tissues. Total RNA isolated from indicated tissues was analysed by RT-qPCR. Data are shown as the mean ± s.d. ($n = 3$). (**d**) The expression of *Foxc1* and *Col2a1* in developing limbs of E12.5 mice was determined by whole-mount *in situ* hybridization. Scale bar, 2 mm (left panel), 1 mm (right panel). (**e**) Haematoxylin and eosin (H&E) staining and *in situ* hybridization analysis of *Col2a1* (middle panel) and *Foxc1* (right panel) in growth plate chondrocytes of E15.5 mice tibia. The boxed area shows higher magnification of distal chondrocytes. Scale bar, 200 μm (lower magnification, × 20) and 100 μm (higher magnification, × 40).

sternum and impaired calcification in vertebrae compared with wild-type (WT) mice (Supplementary Fig. 3a,b). Moreover, *Foxc1*$^{ch/ch}$ mice exhibited significantly shorter limbs than WT (Supplementary Fig. 3c–e). Consistent with this, histological analysis of femurs (Fig. 2a) and tibias (Supplementary Fig. 3f) of newborn mice also showed weaker Alcian Blue staining and a smaller ossification centre in *Foxc1*$^{ch/ch}$ mice compared with WT littermates. Notably, the sternum phenotype was characterized by disorganized rib fusion, the complete absence of hypertrophic chondrocytes and ossification (Fig. 2b). Further analysis of tibial growth plate chondrocytes revealed that the *Foxc1*$^{ch/ch}$ hypertrophic chondrocyte zone was significantly longer than that of WT mice (Fig. 2c,d). These data suggest that Foxc1 inactivation disrupts endochondral ossification, leading to an abnormal skeletal phenotype.

To further investigate endochondral ossification in *Foxc1*$^{ch/ch}$ mice, we investigated embryonic growth plate chondrocytes. *Foxc1*$^{ch/ch}$ mice at E15.5 showed a slight dwarf phenotype and

Table 1 | Ten most highly expressed transcription factors in Venus-positive cells.

	Gene symbol	Definition	Fold change(Log_2) Venus(+)/ Venus(−)	Signal intensity of Venus(+)
1	Sox8	SRY-box containing gene 8	3.7	206
2	Sox6	SRY-box containing gene 6	3.2	906
3	Sox5	SRY-box containing gene 5	3.2	377
4	Runx3	Runt-related transcription factor 3	3.0	213
5	Bhlhe40	Basic helix–loop–helix family	2.9	574
6	Foxc2	Forkhead box c2	2.9	304
7	Sox9	SRY-box containing gene 9	2.7	1601
8	Jdp2	Jun dimerization protein 2	2.6	1657
9	Foxc1	Forkhead box c1	2.5	1284
10	Tcfl5	Transcription factor-like 5	2.5	184

smaller ossification areas (Supplementary Fig. 4a,b), and haematoxylin and eosin (H&E) staining of E15.5 tibias demonstrated degradation of the hypertrophic chondrocyte zone in the centre of WT but not *Foxc1*$^{ch/ch}$ tibias (Fig. 2e). *In situ* hybridization analysis of E15.5 tibias revealed a reduced and delayed *Col10a1*-positive zone in *Foxc1*$^{ch/ch}$ mice compared with that of WT mice, whereas the expression patterns of other chondrocyte genes were unchanged (Fig. 2e). Immunofluorescence analysis also showed a decrease in the Col10-positive area and a delay of Col10 expression in *Foxc1*$^{ch/ch}$ mice compared with that in WT mice (Supplementary Fig. 4c). Moreover, MMP13 expression was markedly diminished (Fig. 2f) and the invasion of *Col1a1*- and *Runx2*-positive osteoblasts was not observed in *Foxc1*$^{ch/ch}$ mice (Supplementary Fig. 4d), suggesting retarded chondrocyte hypertrophy. Collectively, these data suggest that *Foxc1*$^{ch/ch}$ mice exhibit abnormal skeletal development because of a delay in endochondral ossification.

Foxc1 directly regulates *PTHrP* expression. We next examined the functional role of Foxc1 in endochondral ossification. Because Foxc1 protein is expressed in resting, proliferating and hypertrophic chondrocytes (Supplementary Fig. 2b), we reasoned that it must be involved in both early and late stages of endochondral ossification. This idea is consistent with results observed in *Foxc1*$^{ch/ch}$ mice (Fig. 2a–c, Supplementary Fig. 3). To test this, we used RT–qPCR to identify Foxc1 target genes in resting and proliferating chondrocytes. When Foxc1 was overexpressed in primary chondrocytes, it markedly increased *PTHrP* expression (Fig. 3a). Together with our earlier immunohistochemical analysis (Supplementary Fig. 2a), which showed the expression of Foxc1 in perichondrial cells at the end of growth plates, this suggests that *PTHrP* is a target gene of Foxc1 in the early stage of chondrocyte development. In support of this, the *PTHrP* promoter was found to contain a motif that fits the core consensus Foxc1-binding sequence[29] (Fig. 3b). DNA pull-down assays using the biotinylated Foxc1-binding element demonstrated that Foxc1 directly bound to this element and that binding was markedly competed with by excess non-biotinylated probe in a dose-dependent manner (Fig. 3b). Chromatin immunoprecipitation (ChIP) with an anti-Foxc1 antibody showed the direct binding of Foxc1 to the *PTHrP* promoter (Fig. 3c). Moreover, Foxc1 increased the promoter activity of a reporter construct containing six copies of the Foxc1-binding element from the *PTHrP* promoter in a dose-dependent manner (Fig. 3d). Foxc1 was further shown to regulate *PTHrP* expression because mRNA isolated from *Foxc1*$^{ch/ch}$ limbs had reduced levels of *PTHrP* mRNA compared with that from WT limbs (Fig. 3e). Of note, a BrdU labelling assay demonstrated that *Foxc1*$^{ch/ch}$ chondrocytes had a significantly decreased proliferation rate compared with that of WT chondrocytes, suggesting that the Foxc1-dependent PTHrP action in growth plate chondrocytes was impaired in *Foxc1*$^{ch/ch}$ mice (Supplementary Fig. 5). Taken together, these data indicate that *PTHrP* is likely to be a direct target gene of Foxc1 in chondrocytes.

Foxc1 regulates Ihh target gene expression with Gli2. Accumulating evidence shows that Ihh and its major signalling molecule, Gli2, regulate *PTHrP* expression in chondrocytes[15,30]. For example, the targeted disruption of *Gli2* in mice causes a reduction in *PTHrP* expression and abnormal endochondral ossification[17]. These reports led us to hypothesize that Foxc1 associates with Ihh–Gli2 signalling in the regulation of *PTHrP*. We observed no significant difference in *Ihh* mRNA levels between *Foxc1*$^{ch/ch}$ and WT mice (Supplementary Fig. 6a). In addition, the overexpression of Foxc1 had no effect on *Ihh* mRNA levels in the presence or absence of Gli2 (Supplementary Fig. 6b). These data suggest that Foxc1 does not affect Ihh expression. In contrast, the concomitant expression of Foxc1 and Ihh in primary chondrocytes increased *PTHrP* expression to levels higher than that induced by Ihh alone (Fig. 3f). These data suggest a functional cooperation between Foxc1 and intracellular signalling activated by Ihh. Notably, a synergistic effect between Foxc1 and Gli2 was observed to affect *PTHrP* expression in primary chondrocytes (Fig. 3g), while a dominant negative (DN) Gli2 decreased Foxc1-dependent *PTHrP* expression (Fig. 3h). Moreover, immunoprecipitation (IP)-western analysis revealed that Foxc1 physically associates with Gli2 (Fig. 3i). In addition, red fluorescent protein (RFP)-tagged Foxc1 co-localized with Venus-tagged Gli2 in the nucleus (Fig. 3j). Collectively, these data suggest that Foxc1 regulates *PTHrP* expression through its functional and physical interaction with Ihh–Gli2 signalling.

In addition to *PTHrP*, Ihh–Gli2 signalling also directly controls the expression of several genes during endochondral ossification, including *Gli1* and *Ptch1* (ref. 12). Thus, we next determined whether Foxc1, with the involvement of Ihh–Gli2 signalling, modulates *Gli1* and *Ptch1* expression. Although Foxc1 alone failed to increase *Gli1* and *Ptch1* mRNA levels in primary chondrocytes, it could stimulate *Gli1* and *Ptch1* expression induced by Ihh (Fig. 4a,b). Consistent with the *PTHrP* mRNA induction (Fig. 3g), the concomitant overexpression of Foxc1 and Gli2 synergistically increased *Gli1* and *Ptch1* expression levels in primary chondrocytes (Fig. 4c,d). It should be noted that *Gli1* and *Ptch1* expression in *Foxc1*$^{ch/ch}$ tibias was reduced compared with that in WT mice (Fig. 4e,f). Moreover, Foxc1 increased the binding of Gli2 to the Gli-binding element located in the *PTHrP*, *Gli1* (ref. 31) and *Ptch1* (ref. 32) promoters, as shown by ChIP assays using an anti-Gli2 antibody (Fig. 4g–i). Of note, the binding activity of endogenous Gli2 to the Gli-binding element located in the *PTHrP*, *Gli1* and *Ptch1* gene promoters was significantly decreased in *Foxc1*$^{ch/ch}$ chondrocytes compared with that in WT chondrocytes (Supplementary Fig. 7). These results collectively suggest that Foxc1, as a transcriptional partner of Gli2, promotes the expression of Ihh target genes, which, in turn, regulates endochondral ossification.

***Col10a1* is a target gene of Foxc1 in chondrocytes**. Foxc1 is expressed in hypertrophic chondrocytes (Supplementary Fig. 2b); therefore, we next examined its role in the late stage of endochondral ossification. We overexpressed Foxc1 in primary

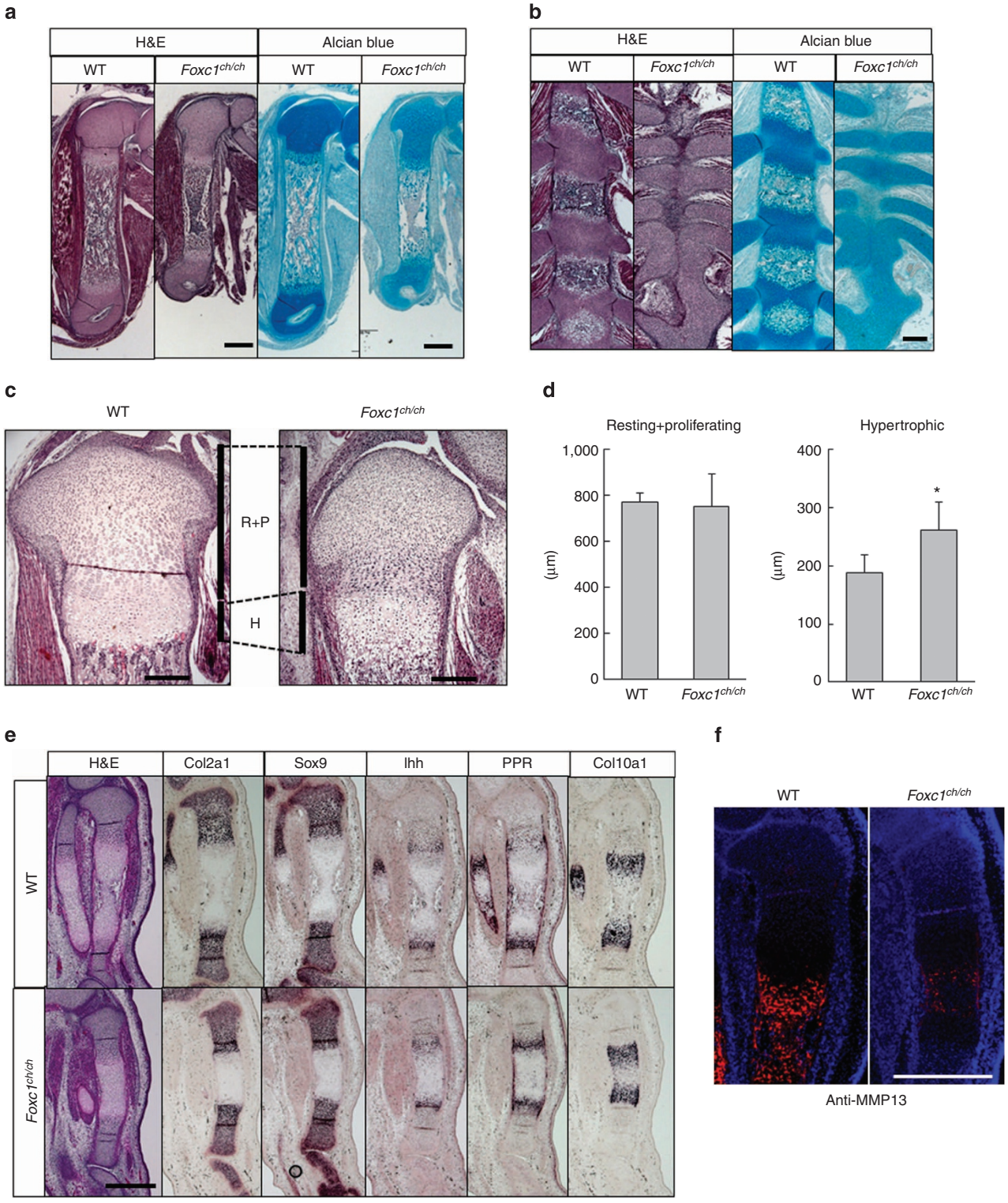

Figure 2 | Delayed endochondral ossification in *Foxc1*$^{ch/ch}$ mice. (**a**,**b**) Histological analysis of newborn WT and *Foxc1*$^{ch/ch}$ littermate femurs (**a**) and sternums (**b**). Paraffin sections of femurs and sternums from newborn WT and *Foxc1*$^{ch/ch}$ littermates were examined by haematoxylin and eosin (H&E) and Alcian blue staining. Scale bar, (**a**) 500 μm. (**b**) 200 μm. (**c**) Histological analysis of tibial growth plate chondrocytes of newborn WT and *Foxc1*$^{ch/ch}$ littermates. H, hypertrophic chondrocytes; P, proliferating chondrocytes; R, resting chondrocytes. Scale bar 200 μm. (**d**) Quantitative analysis of the lengths of the resting and proliferating zone (Resting + Proliferating) and the hypertrophic zone (Hypertrophic) was performed using H&E-stained sections of the tibia. Data are shown as the mean ± s.d. ($n = 6$). *$P < 0.05$ (versus WT); Student's *t*-test. (**e**) Paraffin sections of tibia from E15.5 WT and *Foxc1*$^{ch/ch}$ littermate embryos were examined by H&E staining and *in situ* hybridization using antisense probes against *Col2a1*, *Sox9*, *Ihh*, *PPR* and *Col10a1*. Scale bar, 500 μm. (**f**) Paraffin sections of tibia from E15.5 WT and *Foxc1*$^{ch/ch}$ littermates were subjected to immunofluorescence analyses using an anti-MMP13 antibody. Scale bar, 500 μm.

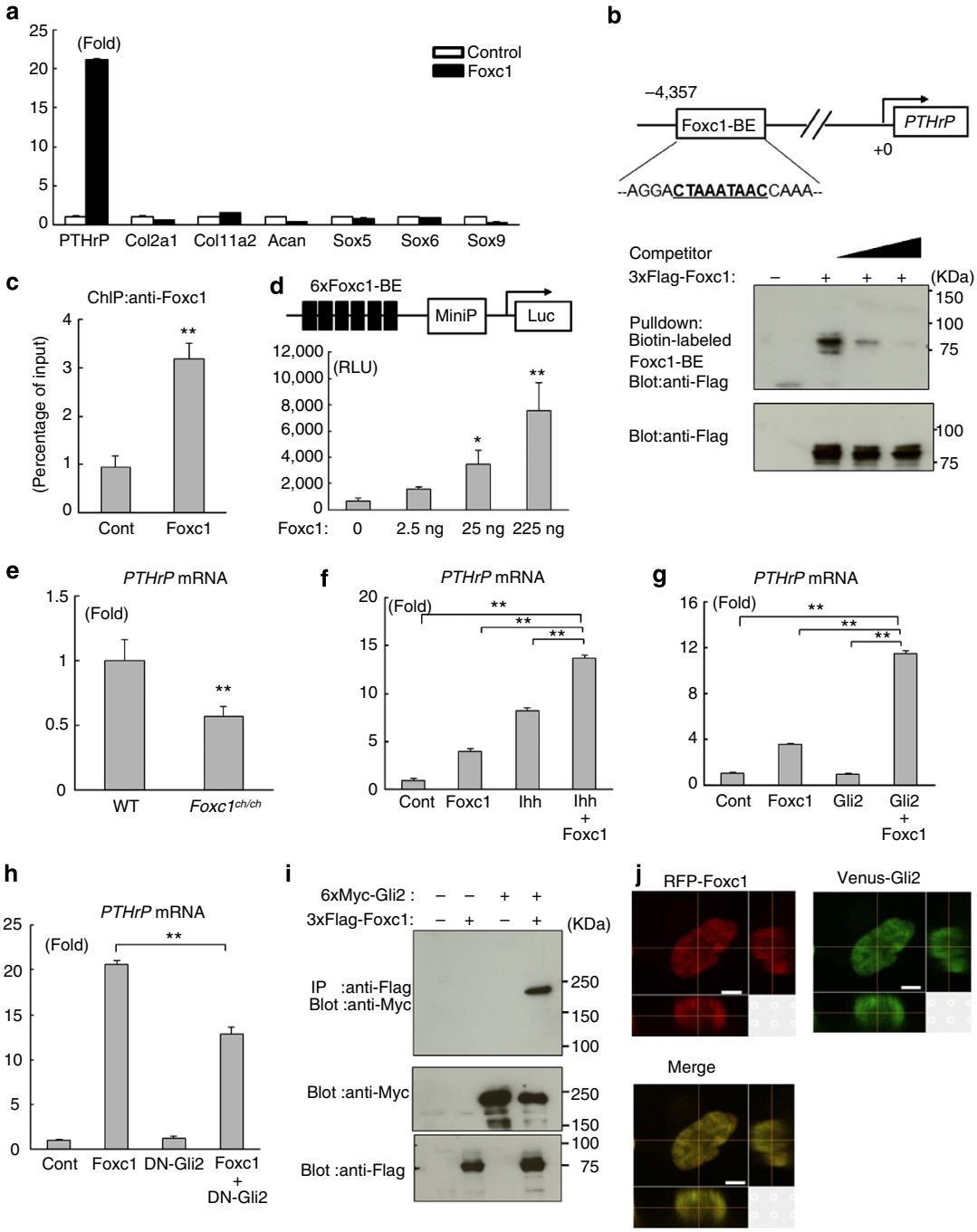

Figure 3 | Foxc1 regulates *PTHrP* expression through physical and functional interaction with Ihh–Gli2 signalling. (**a**) Effects of Foxc1 on chondrocyte gene expression in primary chondrocytes analysed by RT–qPCR. (**b**) DNA pull-down assays using the Foxc1-binding element in the *PTHrP* gene promoter. Schematic presentation of the putative Foxc1-binding element (CTAAATAAC) in the mouse *PTHrP* gene promoter (top panel). 293FT cell lysates precipitated with biotin-labelled Foxc1-BE oligonucleotide (middle panel) and cell lysates (bottom panel) were determined by immunoblotting with an anti-Flag antibody. (**c**) *Foxc1* was overexpressed in primary chondrocytes and ChIP assays were performed using anti-Foxc1 antibody. The binding of Foxc1 to the *PTHrP* gene promoter was examined by qPCR. $^{**}P<0.01$ (versus Control); Student's *t*-test. (**d**) COS-7 cells were transfected with reporter constructs containing 6xFoxc1-BE from the *PTHrP* gene promoter (upper panel) together with an empty vector and Foxc1. RLU, relative luciferase units. $^{*}P<0.05$, $^{**}P<0.01$(versus 0 ng) (**e**) *PTHrP* mRNA expression was determined by RT–qPCR using microdissected hindlimbs isolated from E15.5 $Foxc1^{ch/ch}$ and WT littermate fetuses $^{**}P<0.01$ (versus WT); Student's *t*-test. (**f**,**g**) Synergistic effect of Foxc1 and Ihh (**f**) and Foxc1 and Gli2 (**g**) on *PTHrP* mRNA expression in primary chondrocytes 3 days after infection with the indicated adenoviruses. $^{**}P<0.01$ (versus Control, Foxc1 or Ihh) $^{**}P<0.01$ (versus Control, Foxc1 or Gli2). (**h**) Effect of DN-Gli2 on Foxc1-dependent *PTHrP* mRNA expression in primary chondrocytes 6 days after infection with the indicated adenoviruses; $^{**}P<0.01$ (versus Foxc1). Data for (**a**,**c**,**d**–**h**) are shown as mean ± s.d. ($n=3$) and statistical analysis (**d**,**f**,**g**,**h**) was performed by one-way analysis of variance followed by the Tukey–Kramer test. (**i**) 293FT cell lysates were immunoprecipitated with an anti-Flag antibody and then immunoblotted with an anti-Myc antibody (top panel). The cell lysates were immunoblotted with an anti-Myc (middle panel) or anti-Flag (bottom panel) antibody. (**j**) HEK293 cells were transfected with both RFP-tagged-Foxc1 (RFP-Foxc1) and Venus-tagged Gli2 (Venus-Gli2). Confocal cross sections of *xy* (left), *yz* (right) and *xz* (bottom) were visualized under a confocal microscope. Scale bar, 5 μm.

chondrocytes and evaluated the expression of hypertrophic chondrocyte marker genes. Foxc1 markedly upregulated *Col10a1* expression (Fig. 5a). The *Col10a1* promoter has a putative Foxc1-binding motif in the opposite orientation to that of *Col10a1* transcription (Fig. 5b). DNA pull-down assays using a biotinylated form of this Foxc1-binding element demonstrated

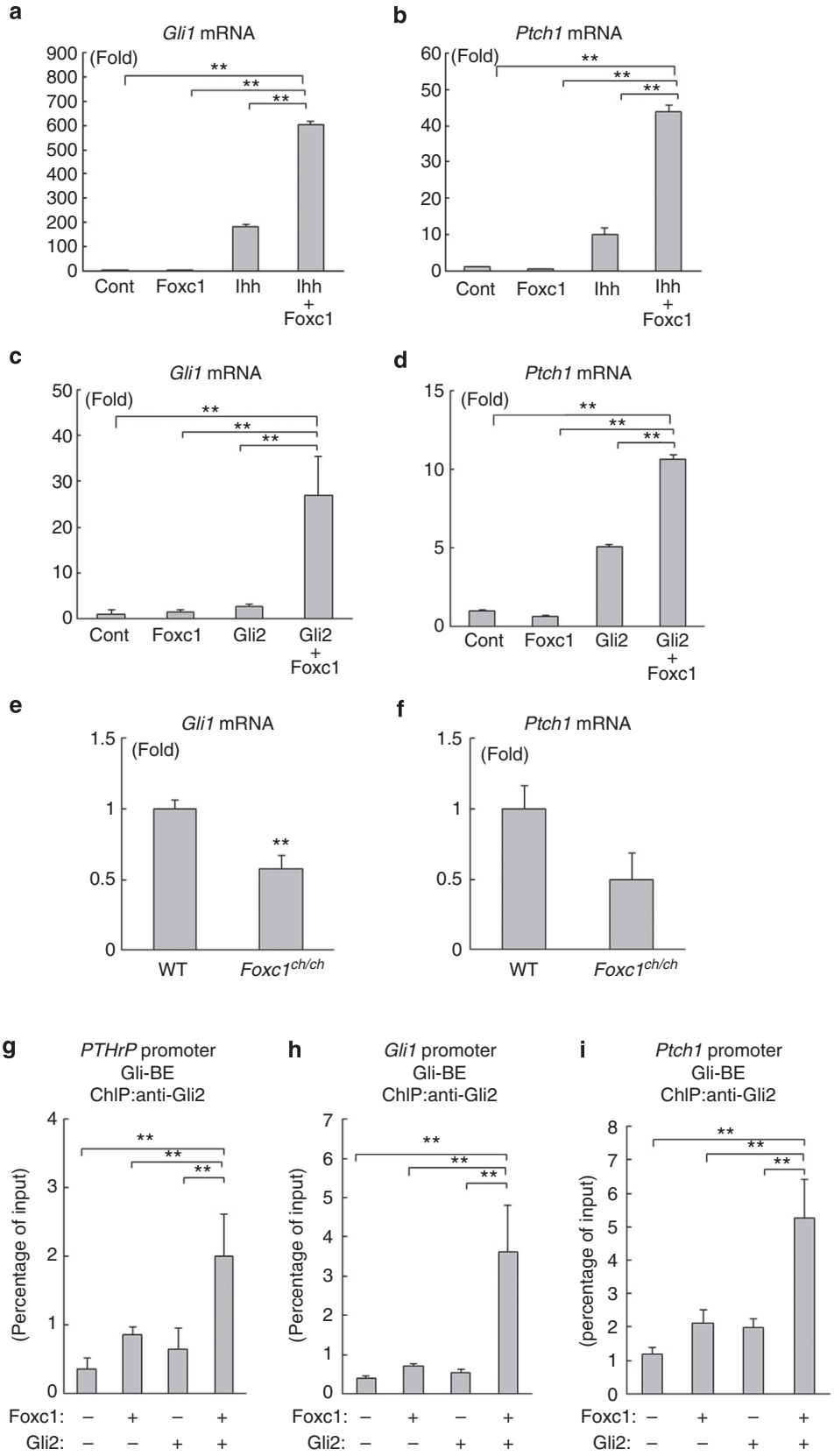

the direct binding of Foxc1, which could be competed with by an excess of non-biotinylated probe (Fig. 5c). ChIP assays using an anti-Foxc1 antibody also revealed that Foxc1 bound to the *Col10a1* promoter (Fig. 5d). Moreover, Foxc1 increased the promoter activity of a reporter construct containing six copies of the *Col10a1* promoter Foxc1-binding element (Fig. 5e), similar to the experiment in Fig. 3d. Taken together, these results suggest that *Col10a1* is a direct target gene of Foxc1 during the late stage of endochondral ossification.

To determine whether Foxc1 regulates *Col10a1* expression during endochondral ossification *in vivo*, we carried out immunofluorescence analysis of tibial growth plates from newborn mice. This revealed that the type-10 collagen-positive zone was significantly shorter in *Foxc1*$^{ch/ch}$ compared with WT mice, while the type-2 collagen-positive zone was unchanged (Fig. 5f,g). In addition, impaired Col10 expression in growth plate chondrocytes was also observed in E15.5 and E17.5 tibia of *Foxc1*$^{ch/ch}$ mice (Supplementary Figs 4c and 8). Analysis of the newborn sternum demonstrated that type-2 collagen-positive chondrocytes failed to undergo sternum development and that type-10 collagen-positive chondrocytes were not detected in *Foxc1*$^{ch/ch}$ mice (Fig. 5h), suggesting impaired chondrocyte hypertrophy. RT–qPCR analysis using primary chondrocytes revealed that *Col10a1* mRNA levels were strikingly decreased in *Foxc1*$^{ch/ch}$ compared with WT mice (Fig. 5i). Importantly, the decrease of *Col10a1* expression in *Foxc1*$^{ch/ch}$ mice was restored by the overexpression of Foxc1 (Fig. 5i). Collectively, these results showed that Foxc1-dependent regulation of *Col10a1* expression is important for endochondral ossification.

DN-Foxc1 reduced Ihh target gene expression. To gain further insight into the role of Foxc1 in chondrogenesis, we examined the effect of a Foxc1 mutant on Ihh target gene expression. We generated a DN mutant of Foxc1 (DN-Foxc1) containing a DNA-binding domain and a transcriptional inhibitory domain[33] (Supplementary Fig. 9a,b). DN-Foxc1 inhibited the transcriptional activity of WT Foxc1 as assessed by a reporter assay (Supplementary Fig. 9c). Overexpression of DN-Foxc1 decreased *PTHrP* and *Col10a1* expression induced by Foxc1 in primary chondrocytes (Supplementary Fig. 9d,e). Of note, DN-Foxc1 also decreased the expression of *PTHrP*, *Gli1*, *Ptch1* and *Col10a1* induced by Ihh (Supplementary Fig. 9f–i). These results indicate the importance of Foxc1 in the chondrogenic action of Ihh.

Functional redundancy between Foxc1 and Foxc2. Although we have shown that Foxc1 controls *PTHrP* expression, which is essential for endochondral ossification, the skeletal phenotype of *Foxc1*$^{ch/ch}$ long bones was relatively mild compared with the severe skeletal defects previously observed in PTHrP-deficient mice[34,35]. Of the forkhead transcription factor superfamily[36], Foxc2 is the most closely related to Foxc1 and Nifuji *et al* reported the expression of Foxc2 in perichondrium[37]. Thus, we reasoned that the mild skeletal defect observed in *Foxc1*$^{ch/ch}$ mice was likely caused by the functional redundancy between Foxc1 and Foxc2. To support this notion, our microarray analysis and RT–qPCR analysis revealed high levels of *Foxc2* expression in chondrogenic cells (Table 1 and Supplementary Fig. 10a). *Foxc2* was also relatively highly expressed in the cartilage tissues of newborn mice (Supplementary Fig. 10b), while immunohistochemical analysis using an anti-Foxc2 antibody revealed Foxc2 expression in resting, proliferating and hypertrophic chondrocytes of the tibial growth plate (Supplementary Fig. 10c). Interestingly, Foxc2 increased *PTHrP* and *Col10a1* expression in primary chondrocytes and stimulated reporter activity through either *PTHrP* or *Col10a1* promoter Foxc1-binding elements (Supplementary Fig. 10d–g). However, the synergistic effects of Foxc2 and Gli2 on Ihh target gene expression, including for *PTHrP*, *Gli1* and *Ptch1*, were significant but very weak (Supplementary Fig. 10h–j) compared with those of Foxc1 (Figs 3g and 4c,d). We next compared the expression level of *Foxc1* and *Foxc2* in chondrocytes. We found stronger expression of *Foxc1* in growth plate chondrocytes compared with that of *Foxc2* as determined by *in situ* hybridization analysis (Supplementary Fig. 11a). RT–PCR analysis also showed a low level of *Foxc2* mRNA in rib cartilage and primary chondrocytes, while the level of *Foxc2* mRNA was approximately equivalent to that of *Foxc1* mRNA in kidney (Supplementary Fig. 11b). Taken together, these data suggest that Foxc2 has a similar function but does not completely overlap with that of Foxc1 in endochondral ossification.

A *Foxc1* missense mutation failed to interact with Gli2. The Axenfeld–Rieger syndrome, characterized by glaucoma, hypodontia and skeletal abnormalities, including facial dysmorphism and short stature, is caused by mutations in *FOXC1* (refs 27,38,39). Interestingly, mutations of *PTHLH*, a human homologue of *PTHrP*, cause brachydactyly and a similar disorder in which patients have a short stature and missing teeth[40]. These clinical observations suggest clinical relevance for the Foxc1–PTHrP axis in the Axenfeld–Rieger syndrome. Thus, we next investigated the pathological role of the *FOXC1* mutation, Phe112Ser (F112S), previously identified in the Axenfeld–Rieger syndrome[26,41]. We confirmed that the expression of the mutant protein F112S was equivalent to that of WT Foxc1 (Fig. 6a). Transfection of the F112S mutant decreased *PTHrP* expression and transcriptional activity of Foxc1, suggesting that F112S acts in a dominant negative manner (Fig. 6b,c). F112S also decreased Ihh-dependent *PTHrP* expression (Fig. 6d). Moreover, the functional interaction between Foxc1 and Gli2 was strikingly attenuated in the F112S transfectant, which, in turn, impaired *PTHrP* induction (Fig. 6e).

Figure 4 | Foxc1 controls the expression of Ihh target genes by recruiting Gli2. (**a**,**b**) Synergistic effect of Foxc1 and Ihh on *Gli1* (**a**) and *Ptch1* (**b**) mRNA expression in primary chondrocytes infected with adenoviruses as indicated. Data are shown as the mean ± s.d. ($n=3$). $^{**}P<0.01$ (versus Control, Foxc1 or Ihh); one-way analysis of variance (ANOVA) followed by the Tukey–Kramer test. (**c**,**d**) Synergistic effect of Foxc1 and Gli2 on *Gli1* (**c**) and *Ptch1* (**d**) mRNA expression in primary chondrocytes infected with adenoviruses as indicated. Data are shown as the mean ± s.d. ($n=3$). $^{**}P<0.01$ (versus Control, Foxc1 or Gli2); one-way ANOVA followed by the Tukey–Kramer test. (**e**,**f**) Total RNA was isolated from the microdissected hindlimbs of E15.5 WT and *Foxc1*$^{ch/ch}$ littermate embryos, and *Gli1* (**e**) and *Ptch1* (**f**) mRNA expression was determined by RT–qPCR. Data are shown as fold expression normalized to WT (mean ± s.d., $n=3$). $^{**}P<0.01$ (versus WT); Student's *t*-test. (**g**–**i**) Primary chondrocytes were infected with control, Foxc1, Gli2 or both Foxc1 and Gli2 adenoviruses and cultured for 3 days. ChIP assays were conducted using an anti-Gli2 antibody and DNA binding to gene promoters was determined by qPCR using primer pairs specific for *PTHrP* (**g**), *Gli1* (**h**) and *Ptch1* (**i**) gene promoters, which contain the Gli-binding element. Data are shown as the mean ± s.d. ($n=3$). $^{**}P<0.01$ (versus control, Foxc1, or Gli2); one-way ANOVA followed by the Tukey–Kramer test.

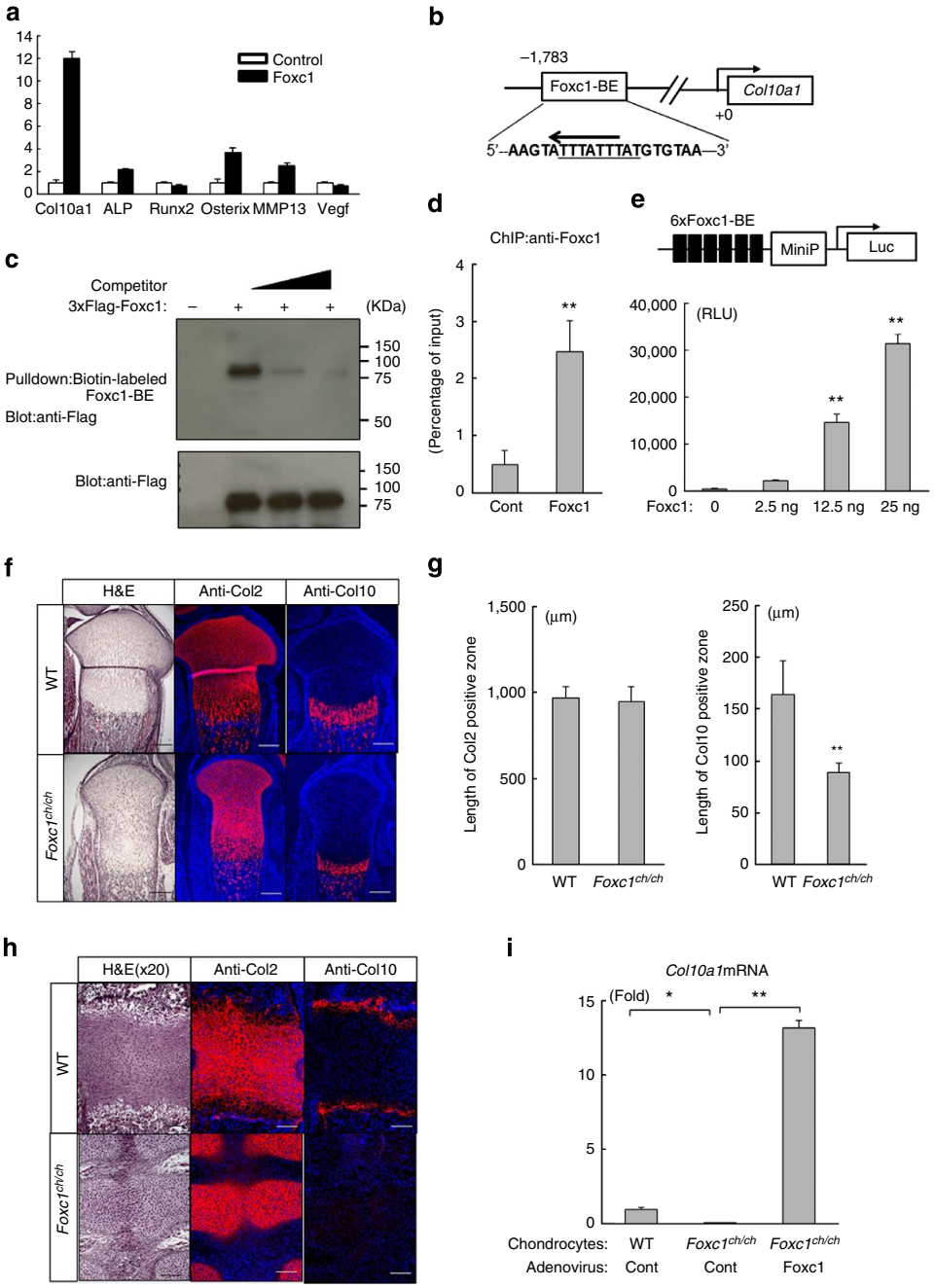

Figure 5 | Col10a1 is the direct target of Foxc1 *in vitro* and *in vivo*. (**a**) Effects of Foxc1 on hypertrophic chondrocyte gene expression. Primary chondrocytes were infected with control or Foxc1 adenovirus and chondrocyte gene expression was analysed by RT-qPCR. Data are shown as the mean ± s.d. ($n=3$). (**b**) Schematic presentation of the putative Foxc1-binding element (ATTTATTTA) in the promoter region of mouse *Col10a1*. (**c**) DNA pull-down assays using the Foxc1-binding element in the *Col10a1* promoter. 293FT cell lysates precipitated with biotin-labelled Foxc1-BE oligonucleotide (upper) and total cell lysates (lower) were assessed by immunoblotting with an anti-Flag antibody. (**d**) ChIP assays using anti-Foxc1 antibody. The binding of Foxc1 to the *Col10a1* promoter was examined by qPCR. Data are shown as the mean ± s.d. ($n=6$). $^{**}P<0.01$ (versus Control); Student's *t*-test. (**e**) COS-7 cells were transfected with reporter constructs containing 6xFoxc1-BE from the *Col10a1* gene promoter (upper panel) together with an empty vector and Foxc1. Data are expressed in relative luciferase units (mean ± s.d., $n=3$). $^{**}P<0.01$ (versus 0 ng); one-way analysis of variance (ANOVA) followed by the Tukey–Kramer test. (**f**) Immunofluorescence analysis of tibial growth plate chondrocytes in newborn WT and *Foxc1*$^{ch/ch}$ littermates. Paraffin sections of tibia were subjected to haematoxylin and eosin (H&E) staining and immunofluorescence analyses using anti-Col2 and anti-Col10 antibodies. Scale bar, 200 μm. (**g**) Quantitative analysis of the lengths of Col2-positive and Col10-positive zones. Data are shown as the mean ± s.d. ($n=5$) $^{**}P<0.01$ (versus WT); Student's *t*-test. (**h**) Immunofluorescence analysis of sternums in newborn WT and *Foxc1*$^{ch/ch}$ mice. Paraffin sections of sternums of the mice were subjected to immunofluorescence analyses using an anti-Col2 or anti-Col10 antibody. The H&E staining images are higher magnification images of those presented in Fig. 2b. Scale bar, 100 μm. (**i**) Primary chondrocytes from E18.5 WT and *Foxc1*$^{ch/ch}$ littermates were infected with control (Cont) or Foxc1 adenovirus as indicated. *Col10a1* mRNA expression was determined by RT-qPCR. Data are shown as the mean ± s.d. ($n=3$) $^{**}P<0.01$, $^{*}P<0.05$; one-way ANOVA followed by the Tukey–Kramer test.

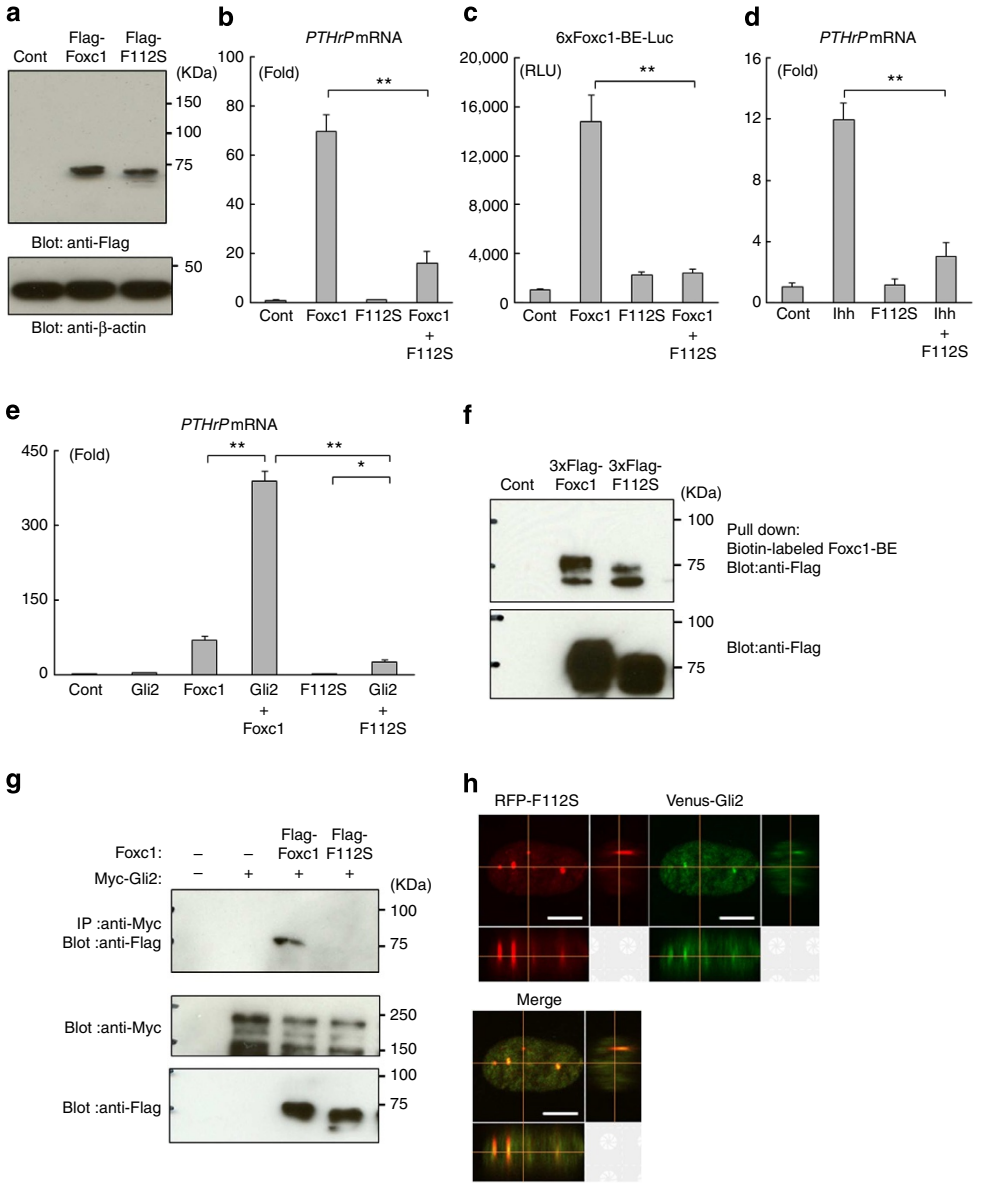

Figure 6 | Impaired functional interaction between a pathological missense *Foxc1* mutant and Gli2. (**a**) 293FT cells were transfected with empty vector, Flag-tagged WT Foxc1 (Flag–Foxc1) or Flag-tagged-F112S mutant Foxc1 (Flag-F112S), and cell lysates were immunoblotted with anti-Flag (upper panel) and anti-β-actin (lower panel) antibodies. (**b**) Effect of F112S mutant on PTHrP. *PTHrP* mRNA expression was determined by RT-qPCR. Data are shown as fold activation normalized to control (mean ± s.d., $n=3$). $^{**}P<0.01$ (versus Foxc1); one-way analysis of variance (ANOVA) followed by the Tukey–Kramer test. (**c**) Effect of the F112S mutation on Foxc1 transcriptional activity on the *PTHrP* promoter. Data are expressed in relative luciferase units (mean ± s.d., $n=3$). $^{**}P<0.01$ (versus Foxc1); one-way ANOVA followed by the Tukey–Kramer test. (**d**) Inhibitory effect of F112S on *PTHrP* mRNA expression induced by Ihh. Data are shown as the mean ± s.d. ($n=3$). $^{**}P<0.01$(versus Ihh); one-way ANOVA followed by the Tukey–Kramer test. (**e**) Impaired synergistic effect between F112S and Gli2 on *PTHrP* mRNA expression. Primary chondrocytes were infected with the indicated adenoviruses and *PTHrP* mRNA expression was analysed by RT-qPCR analysis. Data are shown as the mean ± s.d. ($n=3$). $^{**}P<0.01$, $^{*}P<0.05$; one-way ANOVA followed by the Tukey–Kramer test. (**f**) DNA pull-down assays using the Foxc1-binding element from the *PTHrP* promoter. Samples precipitated with the biotin-labelled Foxc1-BE oligonucleotide (upper panel) and total cell lysates (lower panel) were immunoblotted with an anti-Flag antibody. (**g**) F112S failed to interact with Gli2. Lysates of the 293FT cells transfected as indicated were immunoprecipitated with an anti-Myc antibody and immunoblotted with an anti-Flag antibody (top). The cell lysates were immunoblotted with an anti-Myc (middle) or anti-Flag (bottom) antibody. (**h**) Nuclear localization of F112S and Gli2. HEK293 cells transfected with RFP-tagged F112S (RFP-F112S) and Venus-tagged Gli2 (Venus-Gli2). Confocal cross sections of *xy* (top left), *yz* (right) and *xz* (bottom) were visualized under a confocal microscope. Scale bar, 5 μm.

Although F112S could bind the Foxc1-binding element in the *PTHrP* promoter (Fig. 6f), IP-western analysis demonstrated that F112S failed to physically interact with Gli2 (Fig. 6g). RFP-tagged-Foxc1-F112S localized to the nucleus but showed an abnormal aggregation pattern, which resulted in a marked reduction of nuclear co-localization with Venus-tagged Gli2 (Fig. 6h). Furthermore, F112S failed to recruit endogenous Gli2 to the Gli-binding element located in the *PTHrP*, *Gli1* and *Ptch1* gene promoters (Supplementary Fig. 12). These results collectively suggest that the loss of functional interaction between F112S and Gli2 contribute, at least in part, to the pathogenesis of the Axenfeld–Rieger syndrome.

Discussion

Endochondral ossification is characterized by sequential chondrocyte differentiation including resting, proliferating and hypertrophic processes. Chondrocytes form growth plate layers in which specific marker gene expression is strictly controlled by the communication of various transcription factors. Many details of this transcriptional network remain to be elucidated and to achieve a full understanding of the molecular basis of endochondral ossification it is important to identify and characterize the full repertoire of transcription factors involved.

In this study, we performed FACS-assisted microarray profiling using transgenic mouse embryos that selectively express the Venus gene in developing chondrocytes. We identified Foxc1 as a functional transcription factor selectively expressed in chondrocytes under physiological conditions. Foxc1 has a diverse range of biological functions and is essential for the development of several tissues including the heart, blood vessels[42], kidney and urinary tract[43], the eye[44] and bones[45]. The mechanism by which Foxc1 regulates skeletal development has previously been investigated from the viewpoint of intramembranous bone formation with particular focus on osteoblasts, not endochondral ossification. Thus, several groups have reported the importance of bone morphogenetic protein signalling and Msx2 in Foxc1-dependent calvarial bone development[46–48]. Although Alcian blue-positive nodule formation of mesenchymal cells isolated from *Foxc1*^{lacZ} embryos has been studied[45], the molecular mechanisms by which Foxc1 controls endochondral formation are largely unknown. Our results demonstrated that Foxc1 functionally associates with the Ihh–Gli2 signalling pathway during chondrocyte development. Because Ihh has been reported to regulate not only early chondrogenesis through the induction of *PTHrP* but also chondrocyte hypertrophy in a PTHrP-independent fashion[11,14], our findings of Foxc1-dependent regulation of both *PTHrP* and *Col10a1* are consistent with the multiple functions of Ihh in endochondral ossification. Gli2 is the major signalling molecule that transduces the biological function of the hedgehog family of proteins. Interestingly, similar skeletal abnormalities, including delayed endochondral ossification, defects in the vertebral column, and a reduced tibial length, were also observed in Gli2-deficient mice[17,49]. Importantly, we found that the loss of this functional interaction caused by a missense mutation of *Foxc1* is likely to contribute to the pathogenesis of the Axenfeld–Rieger syndrome. In addition, a DN-Foxc1 diminished chondrogenic action of Ihh. Taken together, our study indicates a novel paradigm; interaction between Foxc1 and Ihh–Gli2 signalling is required for normal skeletal development (Supplementary Fig. 13).

Our screening system did not include a cell expansion step, which has several advantages over gene expression profiling using cultured cells. Cartilage tissues exist in unique physiological conditions that cannot be mimicked *in vitro*. These include a three-dimensional structure, abundant extracellular matrix, the absence of vessels and hypoxia. However, because it is generally accepted that these conditions affect chondrocyte gene expression, our screening system enables us to identify transcription factors that genuinely function *in vivo*. Indeed, Venus-positive cells showed high expression of *Sox5*, *Sox6* and *Sox9*, which are known essential transcription factors involved in chondrogenesis (Table 1). Moreover, several reports have indicated that the combination of tissue-specific reporter mice and FACS-assisted microarray profiling is a useful tool in gene screening. For example, Nakamura *et al.*[50] identified *Wwp2* as a Sox9 target gene in chondrocytes using Sox9-3′ EGFP knock-in mice, while Ieda *et al.*[51] identified three transcription factors that enable the direct reprogramming of dermal fibroblasts into functional cardiomyocytes using the *αMHC* promoter. Although we focused on *Foxc1* in this study, other genes identified by microarray analysis might play important roles in endochondral ossification.

Although we showed that Foxc1 regulates Gli2 function by promoting DNA binding of Gli2 to target gene promoters, details of the mode of action remain to be elucidated. One possibility is that Foxc1 promotes chromatin accessibility as a pioneer factor and thereby regulates gene expression. Pioneer factors are known to open up local chromatin structure through chromatin remodelling, and many forkhead family transcription factors function as pioneer factors[52]. For example, FOXA1 is required for the optimal chromatin conditions needed for the DNA binding and gene expression induced by nuclear receptors, including oestrogen and androgen receptors[53,54]. Because Foxc1 does not contain a functional domain that regulates chromatin remodelling, it might recruit a variety of chromatin-modifying enzymes to regulate gene expression. It would be interesting to further investigate the transcriptional partner(s) of Foxc1 in chondrocytes during endochondral ossification.

Our present results indicate that Foxc1 directly regulates *PTHrP* expression in chondrocytes (Fig. 3). PTHrP is expressed in perichondrial cells and delays chondrocyte hypertrophy by maintaining their proliferation. Our detection of Foxc1 in perichondrial cells (Supplementary Fig. 2a) and in the elongated hypertrophic chondrocyte zone in the tibial growth plate of *Foxc1*$^{ch/ch}$ mice (Fig. 2d) support the important role of the Foxc1–PTHrP axis during endochondral ossification. However, the skeletal phenotype of the sternum in *Foxc1*$^{ch/ch}$ mice showing a complete absence of hypertrophic chondrocytes, is not consistent with PTHrP inhibiting chondrocyte hypertrophy. One explanation for this is that morphogenetic processes that are different between the sternum and long bones influence the phenotype differences. For example, during sternal development, bilateral sternal cartilage bars migrate towards the midline and fuse to form the sternum; this is followed by chondrocyte hypertrophy and ossification[55], suggesting a critical role for cell migration during the development of the sternum. Interestingly, Foxc1 is expressed in the sternum primordium of the E12.5 mouse embryo[45] and several reports indicate that it is involved in the migration of various types of cells, including germ[56], endothelial[57] and breast cancer cells[58]. These data suggest that Foxc1-dependent cell migration also contributes to skeletal development. Reduced cell migration activity could, therefore, partly account for the failure of sternum development in *Foxc1*$^{ch/ch}$ mice (Fig. 2b). We found that Foxc1 is widely expressed in growth plates; therefore, it is likely that Foxc1 has multifunctional roles in several stages of cartilage development.

Foxc1$^{ch/ch}$ mice showed elongation of the hypertrophic chondrocyte zone (Fig. 2c,d), whereas the Col10-positive chondrocyte area was significantly decreased in E15.5 (Supplementary Fig. 4c), E17.5 (Supplementary Fig. 8) and P0 *Foxc1*$^{ch/ch}$ tibia (Fig. 5f,g). There is a discrepancy between these phenotypes because type-10 collagen is a well-established specific marker for hypertrophic chondrocytes. Mechanistically, we speculate that reduced Col10 expression makes hypertrophic chondrocytes functionally immature, and subsequently causes their terminal differentiation to be delayed. To support this notion, MMP13 expression was markedly decreased in *Foxc1*$^{ch/ch}$ mice (Fig. 2f). The extended hypertrophic chondrocyte zone is likely due to impaired terminal differentiation, which causes inhibition of vascular invasion and subsequent replacement with bone. Further analysis is needed to characterize the hypertrophic chondrocytes observed in *Foxc1*$^{ch/ch}$ mice.

Among the forkhead protein family members, Foxc2 is most closely related to Foxc1, suggesting that the two proteins may functionally overlap. In this study, we found that Foxc2 is expressed in growth plate chondrocytes and increases *PTHrP* and

Col10a1 expression in primary chondrocytes (Supplementary Fig. 10). Foxc2-deficient mice also showed skeletal abnormalities[59] and the deletion of both *Foxc1* and *Foxc2* in mice resulted in early embryonic lethality[43]. However, the observed skeletal phenotype of *Foxc1*$^{ch/ch}$ did not perfectly match that of *Foxc2*-deficient mice. For instance, no cleft palate was seen in *Foxc1*$^{ch/ch}$ mice yet this was observed in *Foxc2*-deficient mice together with normal sternum development[59]. Thus, *Foxc1* and *Foxc2* have redundant and diverse roles in cartilage development.

We also showed that the F112S mutation in the forkhead DNA-binding domain, responsible for the Axenfeld–Rieger Syndrome, causes loss of the functional association between Foxc1 and Gli2 (Fig. 6). The F112S mutation leads to abnormal craniofacial development and dental abnormalities[41]; however, the molecular basis of this is unknown. It has been reported that disease-causing missense mutations in the forkhead DNA-binding domain of *FOXC1* cause various effects on the structure and function of Foxc1 (refs 29,60,61). For example, I91S and R127H mutations result in nuclear localization defects, while S82T, S131L and R127H mutations reduce the DNA-binding activity. Because the F112S mutation does not affect DNA binding (Fig. 6f), its clinical consequences are likely to result from the failure of transcriptional machinery complex formation, including the involvement of Gli2. It is possible that F112S disrupts the local protein structure, which, in turn, causes abnormal organization of the functional domain located outside the forkhead domain. Moreover, the electrostatic charge distribution on the protein surface might be altered, affecting protein–protein interactions. Molecular modelling or protein structure analysis of the F112S mutation is necessary to uncover the molecular basis of its effect.

In addition to skeletal abnormalities, human *FOXC1* mutations lead to dental anomalies including missing or small teeth. Interestingly, human *PTHLH* mutations are also reported to cause missing teeth[40]. PTHrP and the PTH/PTHrP receptor are expressed in tooth buds[62,63], and overexpression of a constitutively active PTH/PTHrP receptor in mice causes a reduction in the number of ameloblasts and disorganization of the odontoblast layer[64]. These data collectively suggest that the Foxc1–PTHrP axis is also involved in tooth development, and it will be of interest to elucidate the role of Foxc1 during tooth morphogenesis to help determine the pathogenesis of the dental anomalies observed in the Axenfeld–Rieger syndrome.

In conclusion, we identified a novel function for Foxc1 as a critical transcription factor for endochondral ossification. This function modulates the expression of chondrogenic genes through its physical and functional interaction with Ihh–Gli2 signalling. Our findings contribute to an improved understanding of the molecular mechanisms underlying endochondral ossification and provide new insights into the transcriptional network system of skeletal development.

Methods

Generation of *Col2a1*-venus transgenic mice. Venus cDNA (kindly provided by Dr Atsusi Miyawaki, Lab for Cell Function Dynamics, BSI, RIKEN, Japan) was amplified by PCR and fused to the *Col2a1* promoter. This transgene vector, containing a polyA site, was linearized using *Not*I digestion and used to generate transgenic mice by pronuclear injection. DNA was injected into single-cell BDF1 zygotes to generate transgenic mice. To determine mouse genotypes, genomic DNA isolated from tail biopsies was analysed by PCR using specific primers for Venus cDNA (sense primer: 5′-TGGTGGTGCAAATCAAAGAA-3′, antisense primer: 5′-TAGGCTTTCCACGTCGATCT-3′). All experiments were performed under protocols approved by the Osaka University Graduate School of Dentistry animal committee.

Microarray analysis. We dissected rib cartilage, vertebrae and limb buds from E13.5 Col2a1-Venus-Tg mice and digested the tissues into single cells using 0.1% collagenase and 0.1% trypsin. Venus-positive and Venus-negative cells were sorted with a FACS Aria flow cytometer (Becton-Dickinson, NY, USA) using the manufacturer's instructions. Total RNA was extracted using NucleoSpin RNA II (Macherey-Nagle, Duren, Germany) without a cell expansion step. Microarray analysis was performed using the Affymetrix Mouse Genome 430 2.0 Array according to the manufacturer's protocol (Affymetrix, Santa Clara, CA, USA). Microarray data have been deposited in NCBI Gene Expression Omnibus (http://www.ncbi.nlm.nih.gov/geo/) under the accession number GSE65350.

RT-qPCR. Total RNA was denatured at 65 °C for 5 min and then cDNA was synthesized using a ReverTra Ace qPCR RT Master Mix (TOYOBO, Osaka, Japan). For quantification of mRNA, RT–qPCR amplification was performed using the TaqMan PCR protocol and the ABI StepOne Plus real-time PCR system (Applied Biosystems, Foster city, CA, USA). Primers and TaqMan probes used for amplification are listed in Supplementary Table 2. mRNA expression was normalized to that of β-actin. Data are represented as means ± s.d. ($n = 3$).

Whole-mount *in situ* hybridization. A 594-bp fragment of *Foxc1* was amplified using specific primers (sense primer: 5′-CAGAGCTCCCTCTACAGCTCC-3′, antisense primer: 5′-TCAGAATTTGCTACAGTCATA-3′) and subcloned into a pCR2 TOPO vector (Invitrogen, CA, USA). A 405-bp *Col2a1* fragment subcloned into pBluescript SK vector was kindly provided by Dr Toshihisa Komori (Nagasaki University Dental School, Nagasaki, Japan). Plasmid vectors containing *Foxc1* and *Col2a1* fragments were linearized using BamHI (Foxc1) and EcoRI (Col2a1), respectively. Digoxigenin (DIG)-labelled antisense RNA probes for Foxc1 or Col2a1 were generated with SP6 or T7 RNA polymerase, respectively, and using a DIG RNA Labeling kit (Roche, Basel, Switzerland) according to the manufacturer's instructions.

C57BL/6 mouse embryos (E12.5) were fixed in 4% paraformaldehyde (PFA) in PBS overnight at 4 °C. Samples were hybridized overnight at 70 °C with gene-specific DIG-labelled RNA probes, then washed and incubated with anti-DIG antibody conjugated to alkaline phosphatase (anti-DIG-AP antibody, Roche) at a 1:2,500 (v/v) dilution. Nitroblue tetrazolium and 5-bromo-4-chloro-3′-indolyphosphate p-toluidine were used for signal detection.

***In situ* hybridization.** Tibias from E14.5 or E15.5 mice were fixed in 4% PFA–PBS overnight at 4 °C, embedded in paraffin and cut into 5-μm sections. DIG-labelled single-stranded RNA probes were prepared using a DIG RNA labelling kit (Roche) according to the manufacturer's instructions. The sections were deparaffinized and hybridized with chondrocyte gene-specific DIG-labelled RNA probes for 8 h at 70 °C. The signals were detected with alkaline phosphatase-conjugated anti-DIG-AP antibody at a 1:2,500 (v/v) dilution. Plasmid vectors containing fragments of *Foxc1* (594 bp), *Foxc2* (458 bp), *Col2a1* (405 bp), *Sox9* (456 bp), *Ihh* (579 bp), *Ppr* (779 bp), *Col10a1* (637 bp), *Col1a1* (320 bp) and *Runx2* (634 bp) were linearized using *Xba*I (Ppr), EcoRI (Col2a1, Ihh and Col1a1), BamHI (Foxc1, Foxc2, Col10a1 and Runx2) or NcoI (Sox9), respectively. DIG-labelled antisense RNA probes were generated with SP6 (Ppr and Sox9), T3 (Col2a1, Col1a1 and Runx2) or T7 (Foxc1, Foxc2, Ihh and Col10a1) RNA polymerase using a DIG RNA Labeling kit according to the manufacturer's instructions. These chondrocyte gene probes were kindly provided by Dr Noriyuki Tsumaki (Kyoto University, Kyoto, Japan) and Toshihisa Komori (Nagasaki University Dental School, Nagasaki, Japan).

Immunohistochemical and immunofluorescence analyses. Samples were fixed with 4% PFA–PBS, embedded in paraffin and cut into 4-μm-thick sections. The sections were deparaffinized and stained with Mayer's haematoxylin and eosin. Immunohistochemistry was performed using the following antibodies: anti-Col2 (#7050; Chondrex, WA, USA) at a 1:500 (v/v) dilution, anti-MMP13 (#ab39012; Abcam, Cambridge, UK) at a 1:50 (v/v) dilution and anti-Foxc1 (#ab5079) at a 1:50 (v/v) dilution. Antigen retrieval was performed by heat mediation in a citrate buffer (pH 6) for Foxc1 and 5% hyaluronidase in PBS for 30 min at 37 °C for Col2 and MMP13. Immunoreactivity was visualized with a biotinylated anti-rabbit IgG secondary antibody using the ABC Vectastain kit (Vector Laboratories, CA, USA) and the peroxidase substrate DAB kit (Vector Laboratories), according to the manufacturer's protocols. For immunofluorescence staining, Alexa Fluor 555-conjugated anti-rabbit IgG was used at a 1:500 (v/v) dilution as secondary antibody to visualize immunoreactivity. Counterstaining was performed using 4′,6-diamidino-2-phenylindole.

***Foxc1*$^{ch/ch}$ mice.** *Foxc1*^{ch} (congenital hydrocephalus, ch) heterozygous mice were purchased from the Jackson Laboratory (Bar Harbour, ME, USA) and maintained on a standard 12:12-h light/dark cycle. Homozygous *Foxc1*$^{ch/ch}$ mice were obtained by mating heterozygous *Foxc1*$^{ch/+}$ mice[65]. To determine mouse genotypes, genomic DNA was amplified using a Foxc1-specific primer pair (sense primer: 5′-TATGAGCGTGTACTCGCACCCT-3′; antisense primer: 5′-CGTACCGTTCT CCGTCTTGATGTC-3′) and PCR products were then digested with *Cac*8I (ref. 43). The WT gene yields 178 bp 197 bp fragments and the *Foxc1*^{ch} gene yields a 375 bp fragment. All experiments were performed with E15.5, E17.5 and newborn littermates under protocols approved by the Osaka University Graduate School of Dentistry animal committee.

Skeletal preparation. The skin of newborn and E15.5 mice was removed and fixed with 95% ethanol overnight. Cartilage tissues were stained with 1.5% Alcian blue followed by staining of bone tissues with 0.02% alizarin red. Skeletal preparation samples were photographed under a stereoscopic microscope.

Cell culture and reagents. HEK293, 293FT and COS-7 cells were purchased from the RIKEN Cell Bank (Tsukuba, Japan) or Life Technologies, and cultured in Dulbecco's modified Eagle's medium (Sigma-Aldrich, MO, USA) containing 10% fetal bovine serum at 37 °C in a humidified 5% CO_2 incubator.

Isolation of primary chondrocytes. Mouse primary chondrocytes were isolated according to the protocol described by Gartland *et al.*[66] In brief, the rib cartilage was dissected from newborn mice and digested with 0.1% collagenase D (Roche) and 0.5% trypsin (Life Technologies, CA, USA) for 6 h at 37 °C and then centrifuged for 5 min at 1,500 *g*. The supernatant was removed and the pellet resuspended with α-minimum essential medium containing 10% fetal bovine serum and antibiotics. Cells within two passages were used as primary chondrocytes for experiments.

Construction of expression vectors and transfection. WT and mutant *Foxc1* cDNAs were amplified by PCR and subcloned into the Eco*RI* and Xba*I* sites of an expression vector containing 6 × Myc, Flag and 3 × Flag epitopes. The primer pairs used for PCR were as follows (WT *Foxc1*: sense primer: 5′-GAATTCCAGGCGCG CTACTCGGTGTCC-3′, antisense primer: 5′-TCTAGACTAGAATTTGCTACAG TCATAGAC-3′) (DN-*Foxc1*: sense primer: 5′-GAATTCGACATGGTGAAGCC GCCCTAC-3′, antisense primer: 5′-TCTAGATTAGATGCAGGGTGGTGGCT GGC-3′). RFP-tagged *Foxc1* was generated by subcloning into pTurbo RFP-C (Evrogen, Moscow, Russia). DNA fragments of *Gli2* and DN mutants of *Gli2* (amino acids 2–497) were generated and tagged with the Myc-epitope by subcloning PCR products into pcDNA3 (ref. 67). Transfection of expression vectors was carried out using FuGENE6 (Roche) according to the manufacturer's protocol.

Generation of adenovirus. Recombinant adenoviruses carrying Flag-tagged cDNAs of Foxc1, Flag-tagged DN-Foxc1, Flag-tagged-F112S mutant, Flag-tagged Foxc2, Myc-tagged Gli2 and Myc-tagged DN-Gli2 (ref. 67) was constructed by homologous recombination between the pAxCAwt expression cosmid cassette (Takara Bio, Shiga, Japan) and the parental virus genome in HEK293 cells. The viruses were confirmed to retain no proliferative activity in cells other than HEK293 cells. The expression of proteins was determined by western blotting using anti-Flag antibodies.

Western blotting. Cells were rinsed twice with PBS and solubilized in lysis buffer (20 mM HEPES (pH 7.4), 150 mM NaCl, 1 mM EGTA, 1.5 mM $MgCl_2$, 10% glycerol, 1% Triton-X-100, 10 μg ml^{-1} aprotinin, 10 μg ml^{-1} leupeptin, 1 mM 4-(2-aminoethyl) benzenesulfonyl fluoride hydrochloride, 0.2 mM sodium orthovanadate). The lysates were centrifuged for 10 min at 4 °C at 15,000*g* and boiled in SDS sample buffer containing 0.5 M β-mercaptoethanol for 5 min. Samples were then separated by SDS–polyacrylamide gel electrophoresis, transferred to nitrocellulose membranes, immunoblotted with primary antibodies and visualized with horseradish peroxidase-coupled anti-mouse (1:10,000) or -rabbit(1:5,000) immunoglobulin IgG antibodies using enhanced chemiluminescence detection kits (GE Healthcare, Buckinghamshire, UK). Anti-Flag (#F3165, 1:10,000) antibodies were purchased from Sigma-Aldrich. Anti-Myc (#ab9132, 1:2,000) was purchased from Abcam. Full scans of western blotting data are shown in Supplementary Fig. 14.

Reporter assays. A firefly luciferase reporter construct containing six copies of the *Foxc1*-binding element from the *PTHrP* promoter (5′-CAGCAGGACTAAATAAC CAAATCCT-3′) or from the *Col10a1* promoter (5′-TAAAAGTATTTATTTATG TGTAAGT-3′) was subcloned into pGL4.23 (Promega, WI, USA). Reporter constructs were co-transfected with *Foxc1* expression vectors into COS-7 cells using FuGENE6. Forty-eight hours after transfection, the cells were lysed and luciferase activity was measured using specific substrates in a luminometer (Promega) according to the manufacturer's protocol.

IP-western analysis. Cells transfected with Flag–Foxc1 and Myc–Gli2 were washed three times with ice-cold PBS and solubilized in lysis buffer. The lysates were centrifuged at 15,000 *g* for 20 min at 4 °C and incubated with anti-Flag M2 magnetic beads for 4 h at 4 °C. Immunoprecipitated samples were collected by a magnetic separator and washed five times with ice-cold PBS. Samples were boiled in SDS sample buffer and supernatants were subsequently subjected to western blot analysis.

Confocal microscopy. RFP-tagged WT or RFP-tagged F112S mutant Foxc1 were concomitantly transfected with Venus-tagged Gli2 into HEK293 cells using FuGENE 6. Forty-eight hours after transfection, the cells were fixed with 4% formaldehyde/PBS and washed three times with PBS. Samples were visualized using the Nikon A1 confocal microscope system (Nikon Instech, Tokyo, Japan). The images of *x*–*z* and *y*–*z* stacks were obtained using Nikon NIS-Elements AR software.

DNA pull-down assays. 293FT cells were transfected with Flag–Foxc1 and lysed using lysis buffer (20 mM HEPES (pH 7.4), 150 mM NaCl, 1 mM EGTA, 1.5 mM $MgCl_2$, 10% glycerol, 1% Triton-X-100, 10 μg ml^{-1} leupeptin, 1 mM phenylmethanesulfonyl fluoride, 0.2 mM sodium orthovanadate), then incubated for 3 h with 1 μg of a biotinylated double-stranded oligonucleotide probe containing the Foxc1-binding element present in the *PTHrP* promoter (sense primer: 5′-AGC AGGACTAAATAACCAAATCCTT-3′, antisense primer: 5′-AAGGATTTGGTT ATTTAGTCCTGCT-3′) or in the *Col10a1* promoter (sense primer: 5′-AAAGCT CGAGAATATTGACTGAGATATGAAC-3′, antisense primer: 5′-GTTCATATCT CAGTCAATATTCTCGAGCTTT-3′). Precipitated oligonucleotides were collected using Streptavidin magnetic beads (Dynabeads My One Streptavidin T1, Invitrogen) and washed with lysis buffer. Magnetic beads were resuspended with SDS sample buffer, boiled for 5 min and subjected to western blot analysis.

ChIP assays. ChIP analysis was performed using a ChIP assay kit (ChIP-IT Express; Active Motif, CA, USA) according to the manufacturer's instructions. In brief, the primary chondrocytes infected with Foxc1 or control adenovirus were washed with PBS, and the chromatin was fixed with 1% PFA. Chromatin was prepared and immunoprecipitated with 2 μg anti-Foxc1 (#ab5079) or anti-Gli2 (#ab9132) antibodies (Abcam). DNA fragments were precipitated with protein-A magnetic beads and amplified by PCR using primer pairs specific to the *PTHrP* promoter containing the Foxc1-binding element. Quantitative analysis of ChIP assays was performed with qPCR and relevant primer pairs are listed in Supplementary Table 2.

Statistical analysis. Data were statistically analysed by Student's *t*-test to compare differences between two groups. For more than two groups, we used a one-way analysis of variance or two-way analysis of variance followed by the Tukey–Kramer test. *P* values <0.05 were considered statistically significant.

References

1. Karsenty, G., Kronenberg, H. M. & Settembre, C. Genetic control of bone formation. *Annu. Rev. Cell Dev. Biol.* **25,** 629–648 (2009).
2. Long, F. Building strong bones: molecular regulation of the osteoblast lineage. *Nat. Rev. Mol. Cell Biol.* **13,** 27–38 (2012).
3. Ornitz, D. M. FGF signaling in the developing endochondral skeleton. *Cytokine Growth Factor Rev.* **16,** 205–213 (2005).
4. Kronenberg, H. M. Developmental regulation of the growth plate. *Nature* **423,** 332–336 (2003).
5. de Crombrugghe, B. *et al.* Transcriptional mechanisms of chondrocyte differentiation. *Matrix Biol.* **19,** 389–394 (2000).
6. Maes, C. Role and regulation of vascularization processes in endochondral bones. *Calcif. Tissue Int.* **92,** 307–323 (2013).
7. Krakow, D. & Rimoin, D. L. The skeletal dysplasias. *Genet. Med.* **12,** 327–341 (2010).
8. Pogue, R. & Lyons, K. BMP signaling in the cartilage growth plate. *Curr. Top. Dev. Biol.* **76,** 1–48 (2006).
9. Nishimura, R., Hata, K., Matsubara, T., Wakabayashi, M. & Yoneda, T. Regulation of bone and cartilage development by network between BMP signalling and transcription factors. *J. Biochem.* **151,** 247–254 (2012).
10. Retting, K. N., Song, B., Yoon, B. S. & Lyons, K. M. BMP canonical Smad signaling through Smad1 and Smad5 is required for endochondral bone formation. *Development* **136,** 1093–1104 (2009).
11. Amano, K. *et al.* MSX2 stimulates chondrocyte maturation by controlling Ihh expression. *J. Biol. Chem.* **283,** 29513–29521 (2008).
12. Ingham, P. W. & McMahon, A. P. Hedgehog signaling in animal development: paradigms and principles. *Genes Dev.* **15,** 3059–3087 (2001).
13. Lai, L. P. & Mitchell, J. Indian hedgehog: its roles and regulation in endochondral bone development. *J. Cell Biochem.* **96,** 1163–1173 (2005).
14. Mak, K. K., Kronenberg, H. M., Chuang, P. T., Mackem, S. & Yang, Y. Indian hedgehog signals independently of PTHrP to promote chondrocyte hypertrophy. *Development* **135,** 1947–1956 (2008).
15. St-Jacques, B., Hammerschmidt, M. & McMahon, A. P. Indian hedgehog signaling regulates proliferation and differentiation of chondrocytes and is essential for bone formation. *Genes Dev.* **13,** 2072–2086 (1999).
16. Kesper, D. A., Didt-Koziel, L. & Vortkamp, A. Gli2 activator function in preosteoblasts is sufficient to mediate Ihh-dependent osteoblast differentiation, whereas the repressor function of Gli2 is dispensable for endochondral ossification. *Dev. Dyn.* **239,** 1818–1826 (2010).
17. Miao, D. *et al.* Impaired endochondral bone development and osteopenia in Gli2-deficient mice. *Exp. Cell Res.* **294,** 210–222 (2004).
18. Akiyama, H., Chaboissier, M. C., Martin, J. F., Schedl, A. & de Crombrugghe, B. The transcription factor Sox9 has essential roles in successive steps of the

chondrocyte differentiation pathway and is required for expression of Sox5 and Sox6. *Genes Dev.* **16,** 2813–2828 (2002).
19. Yoshida, C. A. *et al.* Runx2 and Runx3 are essential for chondrocyte maturation, and Runx2 regulates limb growth through induction of Indian hedgehog. *Genes Dev.* **18,** 952–963 (2004).
20. Wuelling, M. & Vortkamp, A. Transcriptional networks controlling chondrocyte proliferation and differentiation during endochondral ossification. *Pediatr. Nephrol.* **25,** 625–631 (2010).
21. Amano, K. *et al.* Arid5a cooperates with Sox9 to stimulate chondrocyte-specific transcription. *Mol. Biol. Cell* **22,** 1300–1311 (2011).
22. Hata, K. *et al.* Paraspeckle protein p54nrb links Sox9-mediated transcription with RNA processing during chondrogenesis in mice. *J. Clin. Invest.* **118,** 3098–3108 (2008).
23. Muramatsu, S. *et al.* Functional gene screening system identified TRPV4 as a regulator of chondrogenic differentiation. *J. Biol. Chem.* **282,** 32158–32167 (2007).
24. Takigawa, Y. *et al.* The transcription factor Znf219 regulates chondrocyte differentiation by assembling a transcription factory with Sox9. *J. Cell Sci.* **123,** 3780–3788 (2010).
25. Hata, K. *et al.* Arid5b facilitates chondrogenesis by recruiting the histone demethylase Phf2 to Sox9-regulated genes. *Nat. Commun.* **4,** 2850 (2013).
26. Nishimura, D. Y. *et al.* The forkhead transcription factor gene FKHL7 is responsible for glaucoma phenotypes which map to 6p25. *Nat. Genet.* **19,** 140–147 (1998).
27. Tumer, Z. & Bach-Holm, D. Axenfeld-Rieger syndrome and spectrum of PITX2 and FOXC1 mutations. *Eur. J. Hum. Genet.* **17,** 1527–1539 (2009).
28. Hong, H. K., Lass, J. H. & Chakravarti, A. Pleiotropic skeletal and ocular phenotypes of the mouse mutation congenital hydrocephalus (ch/Mf1) arise from a winged helix/forkhead transcriptionfactor gene. *Hum. Mol. Genet.* **8,** 625–637 (1999).
29. Saleem, R. A., Banerjee-Basu, S., Murphy, T. C., Baxevanis, A. & Walter, M. A. Essential structural and functional determinants within the forkhead domain of FOXC1. *Nucleic Acids Res.* **32,** 4182–4193 (2004).
30. Vortkamp, A. *et al.* Regulation of rate of cartilage differentiation by Indian hedgehog and PTH-related protein. *Science* **273,** 613–622 (1996).
31. Ikram, M. S. *et al.* GLI2 is expressed in normal human epidermis and BCC and induces GLI1 expression by binding to its promoter. *J. Invest. Dermatol.* **122,** 1503–1509 (2004).
32. Agren, M., Kogerman, P., Kleman, M. I., Wessling, M. & Toftgard, R. Expression of the PTCH1 tumor suppressor gene is regulated by alternative promoters and a single functional Gli-binding site. *Gene* **330,** 101–114 (2004).
33. Berry, F. B., Saleem, R. A. & Walter, M. A. FOXC1 transcriptional regulation is mediated by N- and C-terminal activation domains and contains a phosphorylated transcriptional inhibitory domain. *J. Biol. Chem.* **277,** 10292–10297 (2002).
34. Amizuka, N., Warshawsky, H., Henderson, J. E., Goltzman, D. & Karaplis, A. C. Parathyroid hormone-related peptide-depleted mice show abnormal epiphyseal cartilage development and altered endochondral bone formation. *J. Cell Biol.* **126,** 1611–1623 (1994).
35. Karaplis, A. C. *et al.* Lethal skeletal dysplasia from targeted disruption of the parathyroid hormone-related peptide gene. *Genes Dev.* **8,** 277–289 (1994).
36. Hannenhalli, S. & Kaestner, K. H. The evolution of Fox genes and their role in development and disease. *Nat. Rev. Genet.* **10,** 233–240 (2009).
37. Nifuji, A., Miura, N., Kato, N., Kellermann, O. & Noda, M. Bone morphogenetic protein regulation of forkhead/winged helix transcription factor Foxc2 (Mfh1) in a murine mesodermal cell line C1 and in skeletal precursor cells. *J. Bone Miner. Res.* **16,** 1765–1771 (2001).
38. Chang, T. C., Summers, C. G., Schimmenti, L. A. & Grajewski, A. L. Axenfeld-Rieger syndrome: new perspectives. *Br. J. Ophthalmol.* **96,** 318–322 (2012).
39. Kannu, P., Oei, P., Slater, H. R., Khammy, O. & Aftimos, S. Epiphyseal dysplasia and other skeletal anomalies in a patient with the 6p25 microdeletion syndrome. *Am. J. Med. Genet. A* **140,** 1955–1959 (2006).
40. Klopocki, E. *et al.* Deletion and point mutations of PTHLH cause brachydactyly type E. *Am. J. Hum. Genet.* **86,** 434–439 (2010).
41. Honkanen, R. A. *et al.* A family with Axenfeld-Rieger syndrome and Peters Anomaly caused by a point mutation (Phe112Ser) in the FOXC1 gene. *Am. J. Ophthalmol.* **135,** 368–375 (2003).
42. Kume, T., Jiang, H., Topczewska, J. M. & Hogan, B. L. The murine winged helix transcription factors, Foxc1 and Foxc2, are both required for cardiovascular development and somitogenesis. *Genes Dev.* **15,** 2470–2482 (2001).
43. Kume, T., Deng, K. & Hogan, B. L. Murine forkhead/winged helix genes Foxc1 (Mf1) and Foxc2 (Mfh1) are required for the early organogenesis of the kidney and urinary tract. *Development* **127,** 1387–1395 (2000).
44. Kidson, S. H., Kume, T., Deng, K., Winfrey, V. & Hogan, B. L. The forkhead/winged-helix gene, Mf1, is necessary for the normal development of the cornea and formation of the anterior chamber in the mouse eye. *Dev. Biol.* **211,** 306–322 (1999).
45. Kume, T. *et al.* The forkhead/winged helix gene Mf1 is disrupted in the pleiotropic mouse mutation congenital hydrocephalus. *Cell* **93,** 985–996 (1998).
46. Rice, R., Rice, D. P. & Thesleff, I. Foxc1 integrates Fgf and Bmp signalling independently of twist or noggin during calvarial bone development. *Dev. Dyn.* **233,** 847–852 (2005).
47. Rice, R., Rice, D. P., Olsen, B. R. & Thesleff, I. Progression of calvarial bone development requires Foxc1 regulation of Msx2 and Alx4. *Dev. Biol.* **262,** 75–87 (2003).
48. Mirzayans, F., Lavy, R., Penner-Chea, J. & Berry, F. B. Initiation of early osteoblast differentiation events through the direct transcriptional regulation of Msx2 by FOXC1. *PLoS ONE* **7,** e49095 (2012).
49. Mo, R. *et al.* Specific and redundant functions of Gli2 and Gli3 zinc finger genes in skeletal patterning and development. *Development* **124,** 113–123 (1997).
50. Nakamura, Y. *et al.* Wwp2 is essential for palatogenesis mediated by the interaction between Sox9 and mediator subunit 25. *Nat. Commun.* **2,** 251 (2011).
51. Ieda, M. *et al.* Direct reprogramming of fibroblasts into functional cardiomyocytes by defined factors. *Cell* **142,** 375–386 (2010).
52. Lalmansingh, A. S., Karmakar, S., Jin, Y. & Nagaich, A. K. Multiple modes of chromatin remodeling by Forkhead box proteins. *Biochim. Biophys. Acta* **1819,** 707–715 (2012).
53. Wang, Q. *et al.* A hierarchical network of transcription factors governs androgen receptor-dependent prostate cancer growth. *Mol. Cell* **27,** 380–392 (2007).
54. Carroll, J. S. *et al.* Chromosome-wide mapping of estrogen receptor binding reveals long-range regulation requiring the forkhead protein FoxA1. *Cell* **122,** 33–43 (2005).
55. Kimura, A. *et al.* Runx1 and Runx2 cooperate during sternal morphogenesis. *Development* **137,** 1159–1167 (2010).
56. Mattiske, D., Kume, T. & Hogan, B. L. The mouse forkhead gene Foxc1 is required for primordial germ cell migration and antral follicle development. *Dev. Biol.* **290,** 447–458 (2006).
57. Hayashi, H. & Kume, T. Forkhead transcription factors regulate expression of the chemokine receptor CXCR4 in endothelial cells and CXCL12-induced cell migration. *Biochem. Biophys. Res. Commun.* **367,** 584–589 (2008).
58. Ray, P. S. *et al.* FOXC1 is a potential prognostic biomarker with functional significance in basal-like breast cancer. *Cancer Res.* **70,** 3870–3876 (2010).
59. Iida, K. *et al.* Essential roles of the winged helix transcription factor MFH-1 in aortic arch patterning and skeletogenesis. *Development* **124,** 4627–4638 (1997).
60. Saleem, R. A., Banerjee-Basu, S., Berry, F. B., Baxevanis, A. D. & Walter, M. A. Analyses of the effects that disease-causing missense mutations have on the structure and function of the winged-helix protein FOXC1. *Am. J. Hum. Genet.* **68,** 627–641 (2001).
61. Saleem, R. A., Banerjee-Basu, S., Berry, F. B., Baxevanis, A. D. & Walter, M. A. Structural and functional analyses of disease-causing missense mutations in the forkhead domain of FOXC1. *Hum. Mol. Genet.* **12,** 2993–3005 (2003).
62. Beck, F., Tucci, J., Russell, A., Senior, P. V. & Ferguson, M. W. The expression of the gene coding for parathyroid hormone-related protein (PTHrP) during tooth development in the rat. *Cell Tissue Res.* **280,** 283–290 (1995).
63. Lee, K., Deeds, J. D. & Segre, G. V. Expression of parathyroid hormone-related peptide and its receptor messenger ribonucleic acids during fetal development of rats. *Endocrinology* **136,** 453–463 (1995).
64. Schipani, E. *et al.* Targeted expression of constitutively active receptors for parathyroid hormone and parathyroid hormone-related peptide delays endochondral bone formation and rescues mice that lack parathyroid hormone-related peptide. *Proc. Natl Acad. Sci. USA* **94,** 13689–13694 (1997).
65. Vivatbutsiri, P. *et al.* Impaired meningeal development in association with apical expansion of calvarial bone osteogenesis in the Foxc1 mutant. *J. Anat.* **212,** 603–611 (2008).
66. Gartland, A. *et al. In vitro* chondrocyte differentiation using costochondral chondrocytes as a source of primary rat chondrocyte cultures: an improved isolation and cryopreservation method. *Bone* **37,** 530–544 (2005).
67. Shimoyama, A. *et al.* Ihh/Gli2 signaling promotes osteoblast differentiation by regulating Runx2 expression and function. *Mol. Biol. Cell* **18,** 2411–2418 (2007).

Acknowledgements

We thank Benoit de Crombrugghe (The University of Texas, MD Anderson Cancer Center) for the *Col2a1* gene promoter and Atsushi Miyawaki (RIKEN, BSI) for the Venus construct. We are grateful to Kirsi Sainio (University of Helsinki) for providing *Foxc1*$^{ch/ch}$ mice. This work was supported in part by the Japanese Ministry of Education, Culture, Sports, Science and Technology Grants-in-Aid for Scientific Research (K.H. and R.N.), and 'Challenge to Intractable Oral Diseases' (K.H.), the Uehara Memorial Foundation (K.H. and R.N.), the Senri Life Science Foundation (K.H.), the Nakatomi Foundation (K.H.), and the Mochida Memorial Foundation for Medical and Pharmaceutical Research (K.H.).

Author contributions

K.H and R.N. directed the study. K.H. and M.Y. designed and performed all the *in vitro* and *in vivo* experiments. R.T., E.N., K.O., Y.T. and T.M. performed the molecular and biochemical experiments. S.I., T.T.-Y., and T.Y. discussed and assessed the data. K.H., M.Y. and R.N. wrote the paper.

Additional information

Accession codes: Microarray data have been deposited in the NCBI Gene Expression Omnibus (http://www.ncbi.nlm.nih.gov/geo/) under the accession code GSE65350.

Supplementary Information accompanies this paper at http://www.nature.com/naturecommunications

Competing financial interests: There are no competing financial interests.

Reprints and permission information is available online at http://npg.nature.com/reprintsandpermissions/

How to cite this article: Yoshida, M. *et al.* The transcription factor Foxc1 is necessary for Ihh–Gli2-regulated endochondral ossification. *Nat. Commun.* 6:6653 doi: 10.1038/ncomms7653 (2015).